# EEG correlates of fMRI dynamic functional connectivity states

Afonso Jorge Nunes Aires
afonso.aires@tecnico.ulisboa.pt

Instituto Superior Técnico, Lisboa, Portugal

November 2019

**Abstract**

The brain's intrinsic organization can be assessed by estimating the functional connectivity (FC) between brain regions using functional magnetic resonance imaging (fMRI). Recent studies have shown that FC changes over short time scales of seconds to minutes, naming the so-called dynamic functional connectivity (dFC). Interestingly, dFC has been shown to correlate with brain state, such as eye closure or wakefulness. Moreover, a limited number of recurrent dFC states have been identified. However, the electrophysiological underpinnings of dFC states remain unclear. Here, we examine the electroencephalogram (EEG) correlates of dFC states using simultaneous EEG-fMRI data collected from a group of healthy volunteers. The Phase Coherence method was used to estimate dFC at each repetition time point, TR, and a k-means clustering was then applied to obtain a finite number of dFC states, with a varying k (number of states). For the EEG correlates, the topographies of EEG power across different frequency bands were computed for each TR and a mean topography associated to each dFC state was calculated. Nine dFC states was found to have the best trade-off between low number of states and greater difference between alpha topographies. An association between high power topographies was found with three states, one corresponding to the frontoparietal network, other to the default mode network and the third to a olfactory-middle orbitofrontal network. Our results provide further support to the electrophysiological underpinnings of fMRI dFC states, and in particular indicate a relationship with EEG alpha power.

**Keywords:** functional connectivity, EEG power topography, simultaneous EEG-fMRI, resting-state, dFC states

## 1. Introduction

The study of the human brain activity using Blood Oxygen Level Dependent (BOLD)-functional Magnetic Resonance Imaging (fMRI) revealed correlated and spontaneous low-frequency fluctuations between distant brain regions even without any external stimulus, forming the Resting-state Networks (RSNs) [1]. The brain's intrinsic organization can be assessed by estimating the Functional Connectivity (FC) between brain regions [2]. Initially, it was considered as static. However, recent studies showed that FC fluctuates over short time scales of seconds to minutes, designating the so-called dynamic Functional Connectivity (dFC) [3].

The most common and easiest method used to compute the dFC is the pairwise sliding-window Pearson correlation which consists in computing the Pearson Correlation coefficient within a temporal window with length W and shift the window by a time-step T, repeating this process until the whole time-course has been used [2]. The sliding-window approach can also be used with other FC measures, such as Regional Homogeneity [4] and Independent Component Analysis (ICA) [5], where BOLD time-courses are decomposed through ICA and spatial components are obtained for each window, being possible to observe their evolution over time.

Another family of approaches, which does not use sliding-windows, is the time-frequency analysis, where the Wavelet Transform Coherence is used to estimate time-varying patterns of functional connectivity that are associated with specific frequencies [6].

One last method used to measure dFC is called Phase Synchronization. It is a quite well-established tool in Magnetoencephalography (MEG)/EEG studies, however in fMRI it is not very explored. Glerean and colleagues [7] were one of the first groups to apply it on fMRI and more recently studies have also used it [8, 9], calling it Phase Coherence (PC).

In this method, the purpose is to compute the instantaneous phase, which can be obtained by after computing the analytic signal using the Hilbert transform or by convolving the BOLD signal with a complex Morlet Wavelet. Given the phases of the

BOLD signals from two regions n and p, at time t, the phase coherence, dFC(n,p,t) is computed by:

$$dFC(n,p,t) = \cos(\theta(n,t) - \theta(p,t)) \quad (1)$$

Where cos() refers to the cosine function. When two areas n and p have synchronized BOLD signals at time t, then $dFC(n,p,t) = 1$.

The big advantage of Phase Coherence is that it allows to have a maximum temporal resolution of the dFC, as each dFC matrix is computed at each TR, being possible to analyze faster fluctuations of the FC than using a sliding-window.

A finite number of recurrent dFC patterns can be achieved through matrix factorization techniques. The most commonly used is k-means clustering [4, 8, 10], but others such as Principal Component Analysis [11] or Dictionary learning [12] have been used. One important parameter that needs to be defined *a priori* and has a lot of influence in the results is the number of dFC states. However, this number is not known and and there is not a consensus regarding this number [9].

Furthermore, regarding the dFC states, electrophysiological correlates haven't been much studied to date. In fact, to the best of our knowledge, only Allen and colleagues [13] studied the relationship between dFC states and EEG spectral signatures. The simultaneous EEG-fMRI acquisition has enabled a better understanding of the relationship between haemodynamic and electrical oscillations.

In this study, a dataset acquired with simultaneous EEG-fMRI was used to investigate EEG spectral correlates of dFC states in a resting-state study, in order to understand the electrophysiological underpinnings of these states. Furthermore, it was also investigated if these EEG correlates could be used to solve an old problem of dFC clustering, which is which is the choice of the number of states.

# 2. Materials and Methods

## 2.1. EEG-fMRI Data Acquisition

The dataset analyzed in this work was a simultaneous EEG-fMRI recorded on a 7T MRI scanner using a 64-channel EEG system from nine healthy subjects (22-26 years old, 5 males) [14]. The image acquisitions were performed on an actively-shielded Magnetom 7T/68-cm head scanner (Siemens, Erlangen, Germany). The functional data was acquired using a 2D simultaneous multi-slice gradient-echo echo-planar imaging (EPI) sequence, with a TR = 1 s and a 2.2 mm isotropic resolution. Whole-brain, 1 mm isotropic structural images were acquired using a T1-weighted 3D gradient-echo MPRAGE sequence. Regarding the EEG data, it was acquired using two 32-channel BrainAmp MR Plus amplifiers (Brain Products, Munich, Germany) combined with a BrainCap MR model (EasyCap, Herrsching, Germany). The cap with 64 electrodes was arranged in an extended 10–20 system, with a reference on channel FCz and an electrode used to record the electrocardiogram (ECG) signal, placed on the back of the subject. Scanner triggers marking the onset of each fMRI volume were also recorded.

The fMRI scan was obtained during resting-state and the subjects had to hold eyes open while focusing on a small red cross presented in a MR-compatible LCD screen (Cambridge Research Systems, Rochester, UK), viewed through a mirror placed on the RF coil. This was done to minimize the head and eye movements.

All participants (or their legal representatives) gave written informed consent and the study was approved by the Lausanne's ethics committee.

## 2.2. fMRI Data Analysis

### 2.2.1 Pre-processing

The fMRI data had been previously pre-processed by the team. The first step consisted in discarding the first 10 volumes of the data to let the signal reach a steady-state. Then, non-brain tissue was removed using FMRIB Software Libary (FSL)'s brain extraction tool (BET) [15]. Following this, slice timing and motion correction were accomplished using FSL's motion correction tool (MCFLIRT) [16]. In order to reduce EPI distortions, a B0-unwarp was performed with FSL-TOPUP [17], using a reversed-phase encoding acquisition. Afterwards, a spatial smoothing using a 3 mm full width at half maximum (FWHM) Gaussian kernel was performed and a high-pass temporal filtering with a cut-off period of 100 s was employed. To remove physiological noise, a linear regression with the following regressors was used [18]: quasi-periodic BOLD fluctuations related to cardiac and respiratory cycles were modeled by a fourth order Fourier series using RETROICOR [19]; aperiodic BOLD fluctuations associated with changes in the heart rate as well as in the depth and rate of respiration were convolved with the respective impulse response functions (as reported in [20]); average BOLD fluctuations in white matter (WM) and cerebrospinal fluid (CSF); six motion parameters estimated by MCFLIRT; scan nulling regressors (motion scrubbing) associated with volumes acquired during periods of large head motion.

Afterwards, the T1-weighted structural image of each participant was segmented into gray matter (GM), WM and CSF using Advanced Normalization Tools (ANT)'s tool Atropos [21], to obtain a WM and CSF mask. The functional images were then co-registered into each subject's struc-

tural space using FSL's tool FLIRT and a later co-registration with the Montreal Neurological Institute (MNI) template using FSL's tool FNIRT was done [16, 22]. The following steps were to transform the WM and CSF masks into functional space and erode them with a 3 mm spherical kernel so that partial volume effects were minimized [23]. Moreover, the eroded CSF mask was intersected with a large ventricle's mask from the MNI space, following the rationale described in [20].

The structural image of each participant was parceled into $R = 90$ cortical and sub-cortical non-overlapping region of interest (ROI) according to the Automated Anatomical Labeling (AAL) atlas [24]. Then, these ROIs were co-registered to the patient's functional space and the pre-processed BOLD data was averaged within each ROI.

The following steps were performed in the scope of this Thesis using MATLAB R2016b (The MathWorks Inc., Natick, MA, USA).

#### 2.2.2 Dynamic Functional Connectivity Estimation

The method used to extract these matrices was Phase Coherence (PC). The instantaneous phase of a signal was estimated using the analytic concept of Hilbert transform [8, 9]. The first step consisted in applying a second-order Butterworth band-pass filter in the range 0.01 - 0.1 Hz. Then, the Hilbert transform is applied to the filtered BOLD signal of each ROI $n$ and the phase of each time point, $\theta(n,t)$, is estimated. Afterwards, the dFC is computed for each pair of ROI, $n$ and $p$, using the equation:

$$dFC(n,p,t) = \cos(\theta(n,t) - \theta(p,t)) \tag{2}$$

### 2.3. dFC States Estimation: Leading Eigenvector Dynamics Analysis (LEiDA)

After obtaining the dFC patterns for all time points, the next step is to compare those patterns and identify those that reoccur over time, i.e, summarize the dFC patterns found into a smaller set of connectivity states. In this work, the Leading Eigenvector Dynamics Analysis (LEiDA) [8, 9, 25] was applied which considers only the leading eigenvector of the $N \times N$ dFC matrix at each time point. This allows a big reduction in dimensionality (from $N(N-1)/2$ to $N$ elements), being able to explain the majority of the variance of the BOLD PC (explains over 50% of the variance) [25].

Each eigenvector has $N$ elements (each element corresponds to a brain area) with a positive or negative sign. When all elements of the eigenvector have the same sign, this means that all BOLD phases point in the same direction with respect to the orientation determined by the eigenvector. In this case, a global mode is governing the BOLD signals [9]. On the other hand, when the elements of the eigenvector have different signs, the BOLD signals are following different directions with respect to the leading eigenvector. In this case, the brain areas can be divided in two networks, according to their sign (positive or negative) in the eigenvector. Furthermore, the magnitude of each element of the eigenvector is indicative of the "strength" with each brain area belongs to its community [26], i.e, elements of the eigenvector with higher magnitude indicate brain areas which strongly belong to that network.

Taking advantage of the dimensionality reduction that LEiDA provides and in order to identify the most meaningful dFC patterns (or states) over time, unsupervised learning algorithms are applied, as the dFC states are not known *a priori*. A well known algorithm, applied also in [8, 9, 25] using as input the leading eigenvectors, is the k-means clustering. The algorithm returns a predefined number, k, of centroids ($N \times 1$ vector) that represent each one of the k dFC states. One important issue about the k-means algorithm is that the number of clusters needs to be given *a priori*, even though it is not known.

The k-means algorithm was run with a number of clusters from 3 to 15 using the squared Euclidean distance as the distance metric for minimization. As the algorithm can be stuck in local minima, to try to avoid that the algorithm was run 1000 times and the best result (that where the distance of each cluster point to its centroid was minimum) was chosen.

The classification of each leading eigenvector to a cluster only takes into account the distance between the leading eigenvector and the cluster centroid, and doesn't have a temporal factor so that sudden changes of dFC states (labels) from one time instant to another are not allowed. One way to tackle this problem is by applying a temporal smoothing to the labels in order that each leading eigenvector is not assigned to a cluster centroid only based on the distance to it, but also considering the labels of the nearest leading eigenvectors. Therefore, a smoothing algorithm was implemented in a similar way as Pascual-Marqui and colleagues [27]. In this algorithm, the label of a leading eigenvector is found as the cluster index, k, that minimizes the following distance function:

$$d_{kn}^2 = \|x_n - c_k\|^2 - \lambda b_{kn} \tag{3}$$

where the first portion of the equation refers to the squared Euclidean distance between a leading eigenvector of a time point, $x_n$, and the cluster

centroid $k$, $c_k$, and the second portion corresponds to the temporal smoothing where $\lambda$ denotes how strongly to weigh smoothness and $b_{kn}$ is the amount of time points that have the label k in a window surrounding the n'th sample.

The value chosen for $\lambda$ was 0.5 and the window size was chosen accordingly to the highest frequency present in the BOLD signal, i.e, if the highest frequency is 0.1 Hz , then the window would have a size of $1/0.1 = 10$ s.

## 2.4. EEG Data Analysis

### 2.4.1 Pre-processing

The EEG data pre-processing steps were previously performed as in a previous work by Jorge and colleagues [28]: gradient artifact correction slice-by-slice using Average Artifact Subtraction (AAS) [29]; bad channel interpolation (0–4 per subject); temporal band-pass filtering (1–70 Hz); pulse artifact correction (using a k-means clustering-based approach validated in [14]; downsampling to 500 Hz; motion artifact correction (offline multi-channel recursive least-squares regression using the motion sensor signals [30]); and ICA-based denoising (for removal of gradient and pulse artifact residuals, as well as eyeblink and muscle artifact contributions).

### 2.4.2 Spectral analysis

During the EEG-fMRI acquisition, each fMRI volume was recorded by a scanner trigger, being able to identify the EEG samples corresponding to each TR. So, using this information, the FFT was computed with the number of EEG samples corresponding to each TR period, in order to obtain a spectrum associated to each TR. The FFT was computed to the 59 EEG channels. From the FFT, the power spectral density (or power spectrum) was estimated by taking the magnitude-squared of the FFT.

Then, having in sight the objective of finding an EEG measure that could help differentiate between the dFC states, two measures were computed, for each EEG channel independently. The first was the relative power in EEG bands (delta, theta, alpha and beta), which consists in computing the average power in these bands and divide by the total power. The total power, $TP$, is based on adding the EEG power, $P$, over all frequencies analyzed, which is given by: [31]

$$TP(t) = \sum_{f=1}^{n_f} P(f,t) \tag{4}$$

where $n_f = 20$ Hz, as some artifacts were identified in the power spectrum at some frequencies above 20 Hz, thus these frequencies were not included in the analyses. The average power in the mentioned bands was obtained by dividing the whole band analyzed (1-20 Hz) into four frequency bands: delta [1,4] Hz, theta [4,8] Hz, alpha [8,12] Hz and beta [12,20] Hz. Note that usually the beta band goes up to 30 Hz [32], however due to the reason presented above, the frequency cap is 20 Hz. The average band power at each time point, $BP(t)$, was obtained by summing the power in the corresponding frequency interval:

$$BP(t) = \sum_{f=f_{min}}^{f_{max}} P(f,t) \tag{5}$$

where $f_{min}$ and $f_{max}$ correspond to the minimum and maximum frequency respectively, of each frequency band mentioned above (delta, theta, alpha and beta).

## 2.5. EEG correlates of dFC states

The next step consisted in analyzing the information taken from the EEG combined with the dFC states computed from fMRI data and use that information in the choice of the number of dFC states. Firstly, for each of the approaches presented above, the values from TRs associated with the same dFC state label were averaged, getting a value of that measure for each dFC state, and for each EEG channel. The result is a vector with a dimension of 59, which can represented in space by a topography. The same analysis was done for all number of states computed with the k-means algorithm (3 to 15).

A first analysis encompassed all EEG bands and tried to find one topography that was the most different from all others. However, while comparing the alpha topographies (the band that showed highest differences) for all number of states, it was observed that the assumption that there is one topography different from all others is not entirely true.

This analysis also showed that the most different topographies had higher alpha power than the remaining. So, based on this fact and in order to use a method that did not assume a single state different from the others, but that took into account the possibility of existing more than one topography different from the most but similar to some, the mean of each state topography was computed. This allowed to have a single number characterizing each topography that would reflect the difference between high alpha power and low alpha power. Then, the maximum value was chosen, which, when comparing with the maximum of other states, it would indicate the states that were more associated to alpha power.

In the comparison of each maximum value, the results showed more than one maximum. As a lower number of states is preferred, in order to avoid finding a dFC state too specific of a single subject, the

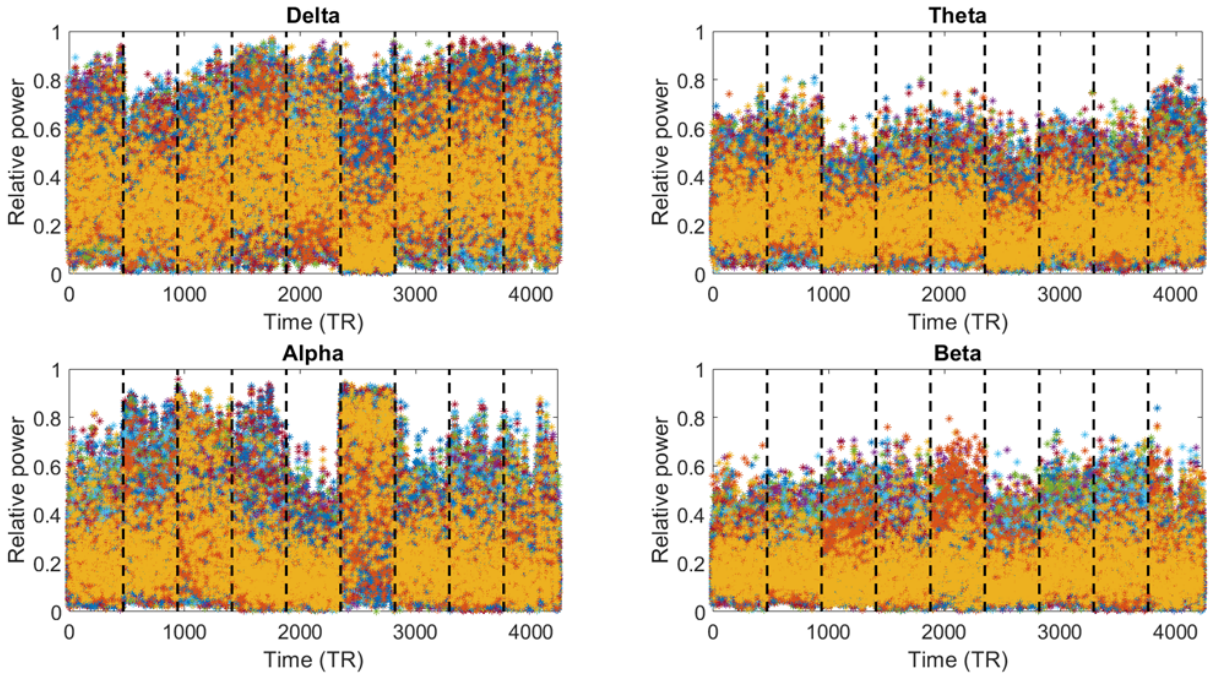


Figure 1: Evolution of relative power in delta, theta, alpha and beta bands over time and subjects. The dashed black lines set the separation between each subject's time-points.

first local maximum was chosen as the number of states k to be analyzed.

dFC states are interpreted as states of in which connectivity across the brain exhibits specific patterns. Although these do not necessarily correspond to the patterns of static (average) connectivity that are found as RSNs, it is nevertheless expectable that some of the dFC states closely resemble RSNs, while other may reflect sub-parts of specific RSNs or combinations of different RSNs.

In order to investigate the similarity of each dFC state with well-established RSNs in the literature, the same procedure used by Lord and colleagues [25] was performed. The 7 RSNs defined in 2 $mm^3$ MNI space by Yeo and colleagues [33] were transformed into 7 vectors with 90 elements each, by counting the number of 2 $mm^3$ MNI voxels in each AAL brain area belonging to each of the 7 networks. As the negative values of the centroid vectors are the ones that represent the network contrasting from the global coherence state, the RSN vectors were transformed to its symmetric so that they could be compared with the centroid vector. Then, the correlation between this vector and the centroid vectors is computed, setting all positive elements in the centroid vectors to zero (elements that belong to the largest network), keeping only the elements with negative sign.

# 3. Results

## 3.1. EEG spectral analysis

The power for each EEG band was obtained through the FFT computed using the time-points between two consecutive TRs for each channel independently. The evolution of the relative power of these bands across time for all subjects and for all channels is represented in figure 1.

Regarding the relative delta power, the distribution of power over time for each subject is identical for all subjects with a small exception for subject 6 where the power is slightly lower than the others. This difference is more pronounced in the relative alpha power, where the power in all time points is relatively higher than in the remaining subjects. One possible explanation could be the inter-individual variability of the power in these bands, i.e, some subjects have naturally more power than others, especially in the alpha band [34]. However, a higher alpha power and consequent lower delta power is characteristic of a higher vigilant state [34]. For any of these reasons, these results imply a more careful analysis in the next results related to the EEG bands.

## 3.2. EEG correlates of dFC states

In order to have a full perspective of the dFC states and the associated alpha topographies, Figure 2

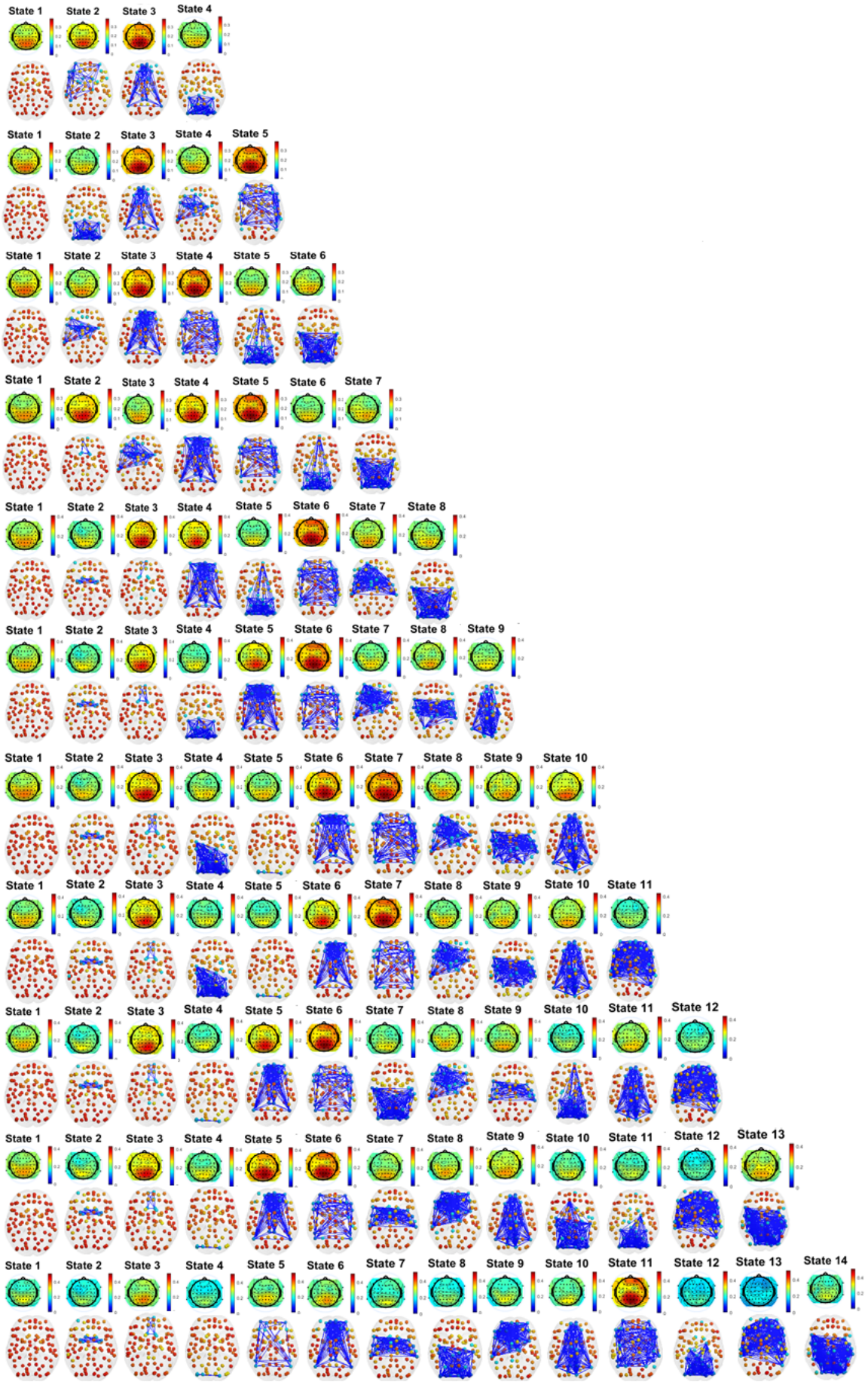


Figure 2: Mean topographies of relative alpha power and cortical representation of the dFC state associated to that topography. The blue links in the cortical representations are plotted between brain regions with a value $< -0.1$.

shows the mean of topographies of relative alpha power across time points with the same dFC label. Due to limitation of space, states from k = 3 and k = 15 were removed.

In Figure 2 it is possible to observe that, aside from 3 states, in all other states the topographies with overall high relative alpha power with a prominence in the central regions of the parietal lobe are associated to at least one of these two networks: one that resembles the default mode network (DMN), with frontal areas, the posterior cingulate cortex and the left and right angular gyrus; another with frontal and parietal regions from the left and right hemispheres, resembling the frontoparietal network. However, the frontoparietal network is the one that has an overall greater power in most states that the others. There is also one more dFC state associated with high alpha power, which appears only with 7 states but maintains until the highest number of states analyzed, that is composed by the middle orbitofrontal gyrus, gyrus rectus and olfactory cortex.

In order to choose a number of states without imposing a number of topographies with high alpha, as these are the most different, the mean value of each topography was computed to characterize each topography by a single value. Then the maximum value was taken in order to select states that have higher alpha than others from different number of states. The comparison between the maximum values obtained on each number of states (3 to 15) are shown in Figure 3.

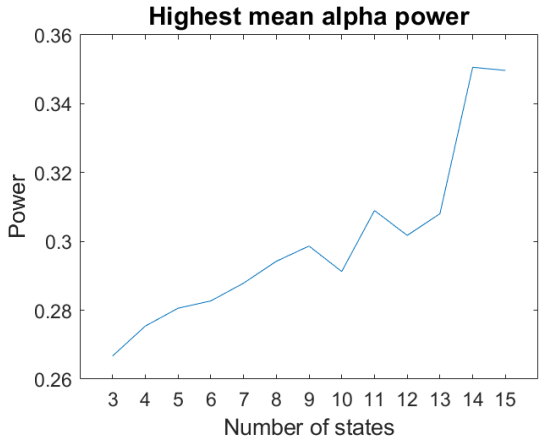


Figure 3: Comparison between the maximum mean of each state topography, for different number of states (3 to 15).

In order to avoid cases where a dFC state is very specific of a single subject, the lowest number of states where there is a local maximum was chosen, that is 9 states. From Figure 2 it is possible to see that state 9 has three states with relatively high alpha power (states 3, 5 and 6).

In order to characterize the states, in specific the three states associated to high alpha power we correlated the centroid vector from all states with the 7 RSN vectors obtained by the transformation of the RSNs defined in [33] into AAL space.

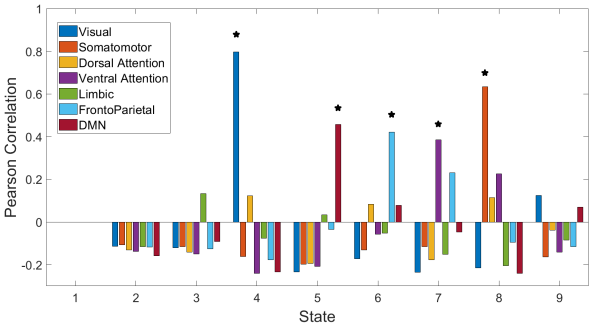


Figure 4: Pearson Correlation between all centroid vectors obtained with K-means clustering for K=9 and the 7 RSNs defined by Yeo and colleagues [33]. The asterisks indicate significant correlations with p-value $< 0.01$.

Figure 4 state 5 is significantly correlated with the DMN ($\mathbf{r} = 0.46$, **p-value** $= 5.9 * 10^{-6}$), state 6 has a significant correlation with the frontoparietal network ($\mathbf{r} = 0.42$, **p-value** $= 3.7 * 10^{-5}$) and state 3 shows no correlation with these RSNs.

# 4. Discussion

The association between dFC states and EEG topographies of alpha power showed three states associated with high alpha power, with a peak on channel Pz and neighbouring channels. Of these three states, one was similar to the DMN, showing a positive correlation with the DMN network extract from Yeo's study [33]; another was similar to the frontoparietal network and the last one was not correlated with any RSN, as it was formed by a small network composed by middle orbitofrontal gyrus, gyrus rectus and olfactory cortex. The association of these states with high alpha was observed for several number of states, highlighting the consistency of this finding.

Regarding the connection between the state similar to the DMN and the increased alpha power, it is, to a certain extent, consistent to a result reported by Allen and colleagues [13], where they found a dFC state (state 3 in their case) that showed a peak in the alpha band in the EEG spectrum, was present during eyes open and had positive correlations between Independent Components (ICs) of the DMN and anti-correlation between DMN and Cognitive Control (CC) regions. However, the DMN regions were also slightly connected to visual ICS, which is not observed in our state. Besides, there were dif-

ferences in the methodologies, as they used ICA to define the ROI instead of using the AAL atlas to segment into ROIs. They also had different conditions on the experiment, since their subjects had their eyes open half of the time and then closed their eyes the other half, while in our study the subjects remained the whole scan with their eyes open. And, finally, they are only analyzing some electrodes (Cz and the combination of O1 and O2), whereas we are using all electrodes. Unfortunately, besides this study, to the best our knowledge, no further studies analysed associations between dFC states and electrophysiological correlates.

A couple studies examined electrophysiological correlates of RSNs [35, 36, 37]. However, in these studies the BOLD time-course of the RSN is known and can be correlated with alpha oscillations, whereas in the case of dFC states, these only show information about the synchronization between brain regions, whether or not the BOLD signal is increasing or decreasing. Thus, only an association between increase of alpha power (alpha synchronization) and dFC states can be elicited from the results.

Concerning the dFC state similar to the frontoparietal network, there is not a state found by Allen and colleagues that has only ICS from this network. The other state, formed by the middle orbitofrontal gyrus, gyrus rectus and olfactory cortex, is an interesting state as only few regions are not synchronized with the global mode. In fact, this highlights one of the main advantages of performing a dFC analysis and also the employment of an atlas (AAL) instead of ICA to choose ICS similar to RSN. As we are not imposing the existence of only resting-state networks, or regions only belonging to them, but are letting the data dictate which brain regions exhibit functional connectivity a greater number of times throughout the scan, this allows to find electrophysiological correlates of brain states that otherwise could have been missed.

The reason these three states are associated with high alpha power mostly on channel Pz and surrounding channels may be related to the proposal of alpha oscillations as an "idling rhythm", i.e, a rhythm whose presence inactivates certain brain regions [38]. High levels of activity of the DMN have been associated to mind wandering and attention lapses [36], being a network that is active when there is no task. Klimesch and colleagues [39] found that alpha synchronization has an active role in performing functional inhibition of regions not relevant to task performance. So, it seems reasonable to have a connection between higher alpha power and higher connectivity between regions of the DMN.

Regarding the frontoparietal network, Sadaghiani and colleagues found that alpha synchronization, i.e, increased alpha power, was positively correlated to cognitive functions associated with the frontoparietal network [40]. Furthermore, a recent study found that this network had a diminished expression after the administration of psilocybin [25]. EEG studies with psilocybin have shown decreased parieto-occipital alpha power [41]. Thus, the association of high alpha power with this network is consistent with these findings.

Regarding state 3, the functionally connected regions that oppose the global mode are regions that are also found connected in the DMN. It may suggest that sub-parts of this network are functionally connected at certain times and at other instants they may connected with other regions. This would, at a certain extent, explain the association of such network with high alpha power. However, further studies need to be performed to understand why high alpha power, mainly parieto-occipital alpha, is associated with these states.

# 5. Conclusions

The main goal of the this study was to analyze EEG spectral correlates of dFC states in order to understand the electrophysiological underpinnings of these states. We concluded that three dFC states, one similar to the frontoparietal network, another to the DMN and a third composed by few frontal regions (the olfactory cortex, middle orbitofrontal gyrus and gyrus rectus) were associated to topographies of increased alpha power, mostly on channel Pz and neighbouring channels.

Regarding the choice of number of states, the EEG revealed to be the decisive factor to this choice. As seen in the results, the number of dFC states associated to distinct alpha power topographies was consistent throughout the majority of the range k = 3 to 15 states. However, if the number of states was, for example, 5 there was one dFC state associated to a high alpha power topography that would be missed. Nonetheless, the criteria to choose the "optimal" number of states still needs to be investigated.

One of the main limitations was the number of subjects. The inter-individual variability of the power in EEG bands [34] in small groups has a lot more influence than if it was performed in a larger group, where this variability would fade away and stronger conclusions could be taken from that analysis. Moreover, some methodological choices should be considered: the use of Hilbert transform to compute the instantaneous phase, mainly at the edges of the BOLD signal, should have further investigations to determine if it is the best method to estimate the phase.

Regarding the clustering with the k-means algo-

rithm, it is not known if it is the best method to cluster the recurrent dFC states, despite being the most used algorithm [4, 8, 10]. And the use of Euclidean distance as the distance measure between clusters is also a parameter to take into account, although Allen and colleagues [10] had similar results using correlation, Euclidean, cosine and L1-norm. Moreover, the dFC labels were smoothed in a window whose size was equal to the inverse of the highest frequency of the band under analysis, however the duration of dFC states is still a matter of debate. Different algorithms for clustering the recurrent dFC states as well as the study of the duration of the dFC states are topics to be explored in future work.

# References


[1] B. Biswal, F. Z. Yetkin, V. M. Haughton, and J. S. Hyde, "Functional connectivity in the motor cortex of resting human brain using echo-planar mri," *Magnetic Resonance in Medicine*, vol. 34, no. 4, pp. 537–541, Oct. 1995. [Online]. Available: https://doi.org/10.1002/mrm.1910340409

[2] M. G. Preti, T. A. Bolton, and D. V. D. Ville, "The dynamic functional connectome: State-of-the-art and perspectives," *NeuroImage*, vol. 160, pp. 41–54, Oct. 2017. [Online]. Available: https://doi.org/10.1016/j.neuroimage.2016.12.061

[3] C. Chang and G. H. Glover, "Time–frequency dynamics of resting-state brain connectivity measured with fMRI," *NeuroImage*, vol. 50, no. 1, pp. 81–98, Mar. 2010. [Online]. Available: https://doi.org/10.1016/j.neuroimage.2009.12.011

[4] A. G. Hudetz, X. Liu, and S. Pillay, "Dynamic repertoire of intrinsic brain states is reduced in propofol-induced unconsciousness," *Brain Connectivity*, vol. 5, no. 1, pp. 10–22, Feb. 2015. [Online]. Available: https://doi.org/10.1089/brain.2014.0230

[5] V. Kiviniemi, T. Vire, J. Remes, A. A. Elseoud, T. Starck, O. Tervonen, and J. Nikkinen, "A sliding time-window ICA reveals spatial variability of the default mode network in time," *Brain Connectivity*, vol. 1, no. 4, pp. 339–347, Oct. 2011. [Online]. Available: https://doi.org/10.1089/brain.2011.0036

[6] M. Yaesoubi, E. A. Allen, R. L. Miller, and V. D. Calhoun, "Dynamic coherence analysis of resting fMRI data to jointly capture state-based phase, frequency, and time-domain information," *NeuroImage*, vol. 120, pp. 133–142, Oct. 2015. [Online]. Available: https://doi.org/10.1016/j.neuroimage.2015.07.002

[7] E. Glerean, J. Salmi, J. M. Lahnakoski, I. P. Jääskeläinen, and M. Sams, "Functional magnetic resonance imaging phase synchronization as a measure of dynamic functional connectivity," *Brain Connectivity*, vol. 2, no. 2, pp. 91–101, Apr. 2012. [Online]. Available: https://doi.org/10.1089/brain.2011.0068

[8] J. Cabral, D. Vidaurre, P. Marques, R. Magalhães, P. S. Moreira, J. M. Soares, G. Deco, N. Sousa, and M. L. Kringelbach, "Cognitive performance in healthy older adults relates to spontaneous switching between states of functional connectivity during rest," *Scientific Reports*, vol. 7, no. 1, Jul. 2017. [Online]. Available: https://doi.org/10.1038/s41598-017-05425-7

[9] C. A. Figueroa, J. Cabral, R. J. T. Mocking, K. M. Rapuano, T. J. Hartevelt, G. Deco, P. Expert, A. H. Schene, M. L. Kringelbach, and H. G. Ruhé, "Altered ability to access a clinically relevant control network in patients remitted from major depressive disorder," *Human Brain Mapping*, vol. 40, no. 9, pp. 2771–2786, Mar. 2019. [Online]. Available: https://doi.org/10.1002/hbm.24559

[10] E. A. Allen, E. Damaraju, S. M. Plis, E. B. Erhardt, T. Eichele, and V. D. Calhoun, "Tracking whole-brain connectivity dynamics in the resting state," *Cerebral Cortex*, vol. 24, no. 3, pp. 663–676, Nov. 2012. [Online]. Available: https://doi.org/10.1093/cercor/bhs352

[11] N. Leonardi, J. Richiardi, M. Gschwind, S. Simioni, J.-M. Annoni, M. Schluep, P. Vuilleumier, and D. V. D. Ville, "Principal components of functional connectivity: A new approach to study dynamic brain connectivity during rest," *NeuroImage*, vol. 83, pp. 937–950, Dec. 2013. [Online]. Available: https://doi.org/10.1016/j.neuroimage.2013.07.019

[12] R. Abreu, A. Leal, and P. Figueiredo, "Identification of epileptic brain states by dynamic functional connectivity analysis of simultaneous EEG-fMRI: a dictionary learning approach," *Scientific Reports*, vol. 9, no. 1, Jan. 2019. [Online]. Available: https://doi.org/10.1038/s41598-018-36976-y

[13] E. A. Allen, E. Damaraju, T. Eichele, L. Wu, and V. D. Calhoun, "EEG signatures of dynamic functional network connectivity states," *Brain Topography*, vol. 31, no. 1, pp. 101–116, Feb. 2017. [Online]. Available: https://doi.org/10.1007/s10548-017-0546-2

[14] J. Jorge, C. Bouloc, L. Bréchet, C. M. Michel, and R. Gruetter, "Investigating the variability of cardiac pulse artifacts across heartbeats in simultaneous EEG-fMRI recordings: A 7t study," *NeuroImage*, vol. 191, pp. 21–35, May 2019. [Online]. Available: https://doi.org/10.1016/j.neuroimage.2019.02.021

[15] S. M. Smith, "Fast robust automated brain extraction," *Human Brain Mapping*, vol. 17, no. 3, pp. 143–155, Nov. 2002. [Online]. Available: https://doi.org/10.1002/hbm.10062

[16] M. Jenkinson, P. Bannister, M. Brady, and S. Smith, "Improved optimization for the robust and accurate linear registration and motion correction of brain images," *NeuroImage*, vol. 17, no. 2, pp. 825–841, Oct. 2002. [Online]. Available: https://doi.org/10.1006/nimg.2002.1132

[17] J. L. Andersson, S. Skare, and J. Ashburner, "How to correct susceptibility distortions in spin-echo echo-planar images: application to diffusion tensor imaging," *NeuroImage*, vol. 20, no. 2, pp. 870–888, Oct. 2003. [Online]. Available: https://doi.org/10.1016/s1053-8119(03)00336-7

[18] R. Abreu, S. Nunes, A. Leal, and P. Figueiredo, "Physiological noise correction using ECG-derived respiratory signals for enhanced mapping of spontaneous neuronal activity with simultaneous EEG-fMRI," *NeuroImage*, vol. 154, pp. 115–127, Jul. 2017. [Online]. Available: https://doi.org/10.1016/j.neuroimage.2016.08.008

[19] G. H. Glover, T.-Q. Li, and D. Ress, "Image-based method for retrospective correction of physiological motion effects in fMRI: RETROICOR," *Magnetic Resonance in Medicine*, vol. 44, no. 1, pp. 162–167, 2000. [Online]. Available: https://doi.org/10.1002/1522-2594(200007)44:1⟨162::aid-mrm23⟩3.0.co;2-e

[20] C. Chang, J. P. Cunningham, and G. H. Glover, "Influence of heart rate on the BOLD signal: The cardiac response function," *NeuroImage*, vol. 44,

no. 3, pp. 857–869, Feb. 2009. [Online]. Available: https://doi.org/10.1016/j.neuroimage.2008.09.029

[21] B. B. Avants, N. J. Tustison, J. Wu, P. A. Cook, and J. C. Gee, "An open source multivariate framework for n-tissue segmentation with evaluation on public data," *Neuroinformatics*, vol. 9, no. 4, pp. 381–400, Mar. 2011. [Online]. Available: https://doi.org/10.1007/s12021-011-9109-y

[22] M. Jenkinson and S. Smith, "A global optimisation method for robust affine registration of brain images," *Medical Image Analysis*, vol. 5, no. 2, pp. 143–156, Jun. 2001. [Online]. Available: https://doi.org/10.1016/s1361-8415(01)00036-6

[23] H. J. Jo, Z. S. Saad, W. K. Simmons, L. A. Milbury, and R. W. Cox, "Mapping sources of correlation in resting state FMRI, with artifact detection and removal," *NeuroImage*, vol. 52, no. 2, pp. 571–582, Aug. 2010. [Online]. Available: https://doi.org/10.1016/j.neuroimage.2010.04.246

[24] N. Tzourio-Mazoyer, B. Landeau, D. Papathanassiou, F. Crivello, O. Etard, N. Delcroix, B. Mazoyer, and M. Joliot, "Automated anatomical labeling of activations in SPM using a macroscopic anatomical parcellation of the MNI MRI single-subject brain," *NeuroImage*, vol. 15, no. 1, pp. 273–289, Jan. 2002. [Online]. Available: https://doi.org/10.1006/nimg.2001.0978

[25] L.-D. Lord, P. Expert, S. Atasoy, L. Roseman, K. Rapuano, R. Lambiotte, D. J. Nutt, G. Deco, R. L. Carhart-Harris, M. L. Kringelbach, and J. Cabral, "Dynamical exploration of the repertoire of brain networks at rest is modulated by psilocybin," *NeuroImage*, vol. 199, pp. 127–142, Oct. 2019. [Online]. Available: https://doi.org/10.1016/j.neuroimage.2019.05.060

[26] M. E. J. Newman, "Finding community structure in networks using the eigenvectors of matrices," *Physical Review E*, vol. 74, no. 3, Sep. 2006. [Online]. Available: https://doi.org/10.1103/physreve.74.036104

[27] R. Pascual-Marqui, C. Michel, and D. Lehmann, "Segmentation of brain electrical activity into microstates: model estimation and validation," *IEEE Transactions on Biomedical Engineering*, vol. 42, no. 7, pp. 658–665, Jul. 1995. [Online]. Available: https://doi.org/10.1109/10.391164

[28] J. Jorge, F. Grouiller, Özlem Ipek, R. Stoermer, C. M. Michel, P. Figueiredo, W. van der Zwaag, and R. Gruetter, "Simultaneous EEG–fMRI at ultra-high field: Artifact prevention and safety assessment," *NeuroImage*, vol. 105, pp. 132–144, Jan. 2015. [Online]. Available: https://doi.org/10.1016/j.neuroimage.2014.10.055

[29] P. J. Allen, O. Josephs, and R. Turner, "A method for removing imaging artifact from continuous EEG recorded during functional MRI," *NeuroImage*, vol. 12, no. 2, pp. 230–239, Aug. 2000. [Online]. Available: https://doi.org/10.1006/nimg.2000.0599

[30] J. Jorge, F. Grouiller, R. Gruetter, W. van der Zwaag, and P. Figueiredo, "Towards high-quality simultaneous EEG-fMRI at 7 t: Detection and reduction of EEG artifacts due to head motion," *NeuroImage*, vol. 120, pp. 143–153, Oct. 2015. [Online]. Available: https://doi.org/10.1016/j.neuroimage.2015.07.020

[31] M. Rosa, J. Kilner, F. Blankenburg, O. Josephs, and W. Penny, "Estimating the transfer function from neuronal activity to BOLD using simultaneous EEG-fMRI," *NeuroImage*, vol. 49, no. 2, pp. 1496–1509, Jan. 2010. [Online]. Available: https://doi.org/10.1016/j.neuroimage.2009.09.011

[32] M. Doppelmayr, W. Klimesch, T. Pachinger, and B. Ripper, "Individual differences in brain dynamics: important implications for the calculation of event-related band power," *Biological Cybernetics*, vol. 79, no. 1, pp. 49–57, Aug. 1998. [Online]. Available: https://doi.org/10.1007/s004220050457

[33] B. T. T. Yeo, F. M. Krienen, J. Sepulcre, M. R. Sabuncu, D. Lashkari, M. Hollinshead, J. L. Roffman, J. W. Smoller, L. Zöllei, J. R. Polimeni, B. Fischl, H. Liu, and R. L. Buckner, "The organization of the human cerebral cortex estimated by intrinsic functional connectivity," *Journal of Neurophysiology*, vol. 106, no. 3, pp. 1125–1165, Sep. 2011. [Online]. Available: https://doi.org/10.1152/jn.00338.2011

[34] M. Jobert, H. Schulz, P. Jähnig, C. Tismer, F. Bes, and H. Escola, "A Computerized Method for Detecting Episodes of Wakefulness During Sleep Based on the Alpha Slow-Wave Index (ASI)," *Sleep*, vol. 17, no. 1, pp. 37–46, 01 1994. [Online]. Available: https://doi.org/10.1093/sleep/17.1.37

[35] E. Tagliazucchi, F. von Wegner, A. Morzelewski, V. Brodbeck, and H. Laufs, "Dynamic BOLD functional connectivity in humans and its electrophysiological correlates," *Frontiers in Human Neuroscience*, vol. 6, 2012. [Online]. Available: https://doi.org/10.3389/fnhum.2012.00339

[36] J. Mo, Y. Liu, H. Huang, and M. Ding, "Coupling between visual alpha oscillations and default mode activity," *NeuroImage*, vol. 68, pp. 112–118, Mar. 2013. [Online]. Available: https://doi.org/10.1016/j.neuroimage.2012.11.058

[37] D. Mantini, M. G. Perrucci, C. D. Gratta, G. L. Romani, and M. Corbetta, "Electrophysiological signatures of resting state networks in the human brain," *Proceedings of the National Academy of Sciences*, vol. 104, no. 32, pp. 13 170–13 175, Aug. 2007. [Online]. Available: https://doi.org/10.1073/pnas.0700668104

[38] G. Pfurtscheller, A. Stancák, and C. Neuper, "Event-related synchronization (ERS) in the alpha band — an electrophysiological correlate of cortical idling: A review," *International Journal of Psychophysiology*, vol. 24, no. 1-2, pp. 39–46, Nov. 1996. [Online]. Available: https://doi.org/10.1016/s0167-8760(96)00066-9

[39] W. Klimesch, P. Sauseng, and S. Hanslmayr, "Eeg alpha oscillations: The inhibition–timing hypothesis," *Brain Research Reviews*, vol. 53, no. 1, pp. 63 – 88, 2007. [Online]. Available: http://www.sciencedirect.com/science/article/pii/S016501730600083X

[40] S. Sadaghiani, R. Scheeringa, K. Lehongre, B. Morillon, A.-L. Giraud, M. D'Esposito, and A. Kleinschmidt, "Alpha-band phase synchrony is related to activity in the fronto-parietal adaptive control network," *Journal of Neuroscience*, vol. 32, no. 41, pp. 14 305–14 310, Oct. 2012. [Online]. Available: https://doi.org/10.1523/jneurosci.1358-12.2012

[41] M. Kometer, A. Schmidt, L. Jancke, and F. X. Vollenweider, "Activation of serotonin 2a receptors underlies the psilocybin-induced effects on oscillations, n170 visual-evoked potentials, and visual hallucinations," *Journal of Neuroscience*, vol. 33, no. 25, pp. 10 544–10 551, Jun. 2013. [Online]. Available: https://doi.org/10.1523/jneurosci.3007-12.2013